



Novel 1,2,4-triazole analogues as mushroom tyrosinase inhibitors: synthesis, kinetic mechanism, cytotoxicity and computational studies

Balasaheb D. Vanjare¹ · Prasad G. Mahajan¹ · Nilam C. Dige² · Hussain Raza² · Mubashir Hassan³ · Yohan Han² · Song Ja Kim² · Sung-Yum Seo² · Ki Hwan Lee¹

Received: 31 January 2020 / Accepted: 29 April 2020
© Springer Nature Switzerland AG 2020

Abstract

We have created a novel series of mushroom tyrosinase inhibitors with 1,2,4-triazole as fundamental skeleton. The target compound 1,2,4-triazol-3-ylthio)-*N*-phenyl acetamide derivatives **9(a–l)** were synthesized by the reaction of 4- and 5-substituted 1,2,4-triazole-3-thiol derivatives **6(a–c)** with 2-chloro-*N*-sub/un-substituted phenyl acetamide derivatives **8(a–d)** under basic condition. By using the analytical techniques for instance, FTIR, LC–MS, ¹H NMR and ¹³C NMR, the structural verification was evaluated. The novel series of the target compounds **9(a–l)** has been scanned for biological activity (mushroom tyrosinase inhibition potential) which demonstrates adequate results. Interestingly, compound **9k** (IC₅₀ = 0.0048 ± 0.0016 μM) exhibits 3500 times more activity compared with standard drug kojic acid (IC₅₀ = 16.8320 ± 1.1600 μM) against mushroom tyrosinase inhibitor. Furthermore, the cytotoxicity experiment was carried out for the highly effective target compounds (**9d**, **9i**, **9j** and **9k**) by using MTT assay method for A375 human melanoma cells to define the nontoxic performance of the most effective compounds ranging from 1 to 25 μM. Furthermore, the molecular docking study delivers the thought concerning the interface of the ligand with an enzyme. Also, the dynamic simulation was accomplished for compound **9k** to govern the plausible binding model.

Keywords 1,2,4-Triazole · Tyrosinase activity · Cytotoxicity · Molecular docking · Dynamic simulation

Introduction

Heterocyclic compounds are extensively dispersed in nature as they perform a major part in the metabolic system which is important for the living things [1–5]. In addition, owing to their different assets, these compounds are observed in many segments, including medicine, agriculture, polymer and material science [5–10]. Thus, the maximum research

groups are presently working on the synthesis and biological application of heterocyclic compounds. One of the vital groups of heterocyclic compounds holding three nitrogen atoms within the five-membered ring is recognized as triazole [11–13]. It covers two kinds of isomer with variation in their virtual arrangement of the three nitrogen atoms within the five-membered ring, for instance, 1,2,3 and 1,2,4-triazoles. Here, in this research work, we are focusing on the synthesis of the 1,2,4-triazole skeleton.

Nowadays, a lot of articles are offered in the synthesis of the Schiff base, natural products and heterocyclic compounds, exhibiting biological activity which belongs to this class [14–17]. Besides, 1,2,4-triazole is one of the extremely considerable scaffolds that can be accountable in the field of the pharmaceutical chemistry which offers a disparity of the biological actions: for instance, anti-inflammatory [18], anticancer [19], antihypertensive [20], antimalarial [21], antibiotic [22], anti-HIV [23, 24], and tyrosinase PDGF-RTK inhibiting agents [25]. Additionally, there are numerous drugs which are available in the market that have triazole core, such as fluconazole used as an antifungal [26];

Electronic supplementary material The online version of this article (<https://doi.org/10.1007/s11030-020-10102-5>) contains supplementary material, which is available to authorized users.

✉ Ki Hwan Lee
khlee@kongju.ac.kr

¹ Department of Chemistry, Kongju National University, Gongju, Chungnam 32588, Republic of Korea

² Department of Biological Sciences, Kongju National University, Gongju, Chungnam 32588, Republic of Korea

³ Institute of Molecular Biology and Biotechnology, The University of Lahore, Lahore 54590, Pakistan

ribavirin used as an antiviral [27]; anastrozole, letrozole used as an antineoplastic [28]; trazodone used as an antidepressant [29]; and rilmazafon used as anxiolytic [30].

Tyrosinase is a copper-containing metalloenzyme that plays a crucial role in the biosynthesis of melanin from tyrosine by the process known as melanogenesis. It is primarily observed in the plant, microorganism and animal tissue [31–35]. It is participating in the first two steps of the melanin biosynthesis: (1) conversion of monophenol into ortho-diphenol by the ortho-hydroxylation and (2) oxidation of the catechol to the ortho-quinone [36]. In brief, the melanin and additional pigments are formed from the tyrosine by the oxidation process catalysed by tyrosinase under various conditions, which is known as melanogenesis. Also, all the processes are carried out in specific organelles and melanosomes in the melanocytes. The real skin colour is determined by the melanin's circulation pattern. Likewise, melanin performs a critical part in absorbing the free radical and in shielding skin from UV rays. Moreover, excessive melanin formation generates various harmful impacts on the skin, for example cancer, melasma, solar lentigo and post-inflammatory melanoderma [37–39]. Therefore, to regulate the melanin synthesis and to cure dermatological-related disease, it is very much valuable to synthesize or to create such an inhibitor, which should not be injurious or not cause further side effects to health.

To conclude, we have developed and produced a series of 12 new 1,2,4-triazole founded derivatives with good yield. All the synthesized derivatives were examined for inhibitory activity of mushroom tyrosinase. From the in vitro report, it has been noticed that all the compounds demonstrate the decent result for the tyrosinase inhibition ranging from ($IC_{50} = 0.0048 \pm 0.0016 \mu\text{M}$) to ($IC_{50} = 0.6545 \pm 0.0988 \mu\text{M}$). Besides, compound **9k** ($IC_{50} = 0.0048 \pm 0.0016 \mu\text{M}$) displayed an outstanding outcome for the inhibition compared with other synthesized derivatives as well as with standard drug kojic acid ($IC_{50} = 16.8320 \pm 1.1600 \mu\text{M}$). In addition, it is very important to clarify the toxic influence of the potent compounds. Therefore, we have screened the most potent target compounds (**9d**, **9i**, **9j** and **9k**) for the cytotoxicity experiment by using MTT assay for A375 human melanoma cells. The results reveal nontoxic performance of **9d**, **9i**, **9j** and **9k** triazole derivatives as compared with nontreated cells even at high concentration ranging from 1 to 25 μM . In addition, the molecular docking reports provide an insight to the enzyme–inhibitors interaction. Also, the molecular dynamic simulation supplied supportive data for complex inhibition of compound **9k** by recognizing binding residues in the vicinity of the binding pocket.

Results and discussion

Chemistry

Design approach

In this investigation, we have manufactured 12 novel 1,2,4-triazole derivatives by modifying several structural aspects of the previously defined tyrosinase inhibitors [40–42]. The advanced structural features designed in our target compounds are shown in Fig. 1. From the literature survey, we come to know that Xie et al. synthesized several novel kojic acid correspondents' derivatives which are screened for the tyrosinase inhibition study. The results expose that derivatives in which the 4-position is substituted with different benzyl amino and benzylidene amino groups in a 1,2,4-triazole core successfully inhibit the tyrosinase activity [41]. Further, in the potential tyrosinase inhibitors, the *N*-(3-(3-(9-methyl-9*H*-carbazol-3-yl) acryloyl) phenyl)-substituted amide functionality was replaced with different substituted phenyl acetamides [40]. After all, established on the bioisosterism auxiliary hypothesis, we have incorporated two distinct scaffolds to originate new scaffold, which was exploited for the tyrosinase inhibition study. The fragment-founded synthetic strategy in the present studies is shown in Fig. 1.

Synthesis

The synthesis path towards the synthesis of the intermediates **2(a–b)**, **3(a–b)**, **5(a–c)**, **6(a–c)**, halogen-substituted/unsubstituted 2-chloro-*N*-phenyl acetamide derivatives **8(a–d)** and the target compounds of 4-, 5-substituted 1,2,4-triazol-3-ylthio)-halogen sub/unsubstituted *N*-phenyl acetamide **9(a–l)** is outlined in Scheme 1. The 3, 4 and 5-substituted 1,2,4-triazole-3-thiol derivatives **6(a–c)** were synthesized by using benzoic acid and 2-fluorobenzoic acid as one of the beginning raw materials. Firstly, sub/unsubstituted benzoic acid derivatives **1(a–b)** are converted into their corresponding ester derivatives **2(a–b)** at reflux temperature under acidic condition. Further, the nucleophilic substitution reaction with hydrazine hydrate in ethanol at reflux state was carried out for the synthesis of the corresponding hydrazide derivative **3(a–b)**. Afterwards, the hydrazide derivatives were condensed with distinct isothiocyanate functionality to form an open-ring intermediate **5(a–c)** under inert atmosphere with acceptable yield which was taken as such for further reaction. The open-ring intermediate **5(a–c)** was cyclised, when refluxed under basic condition to form one of the prerequisite key intermediates termed as a 1,2,4-triazole-3-thiol

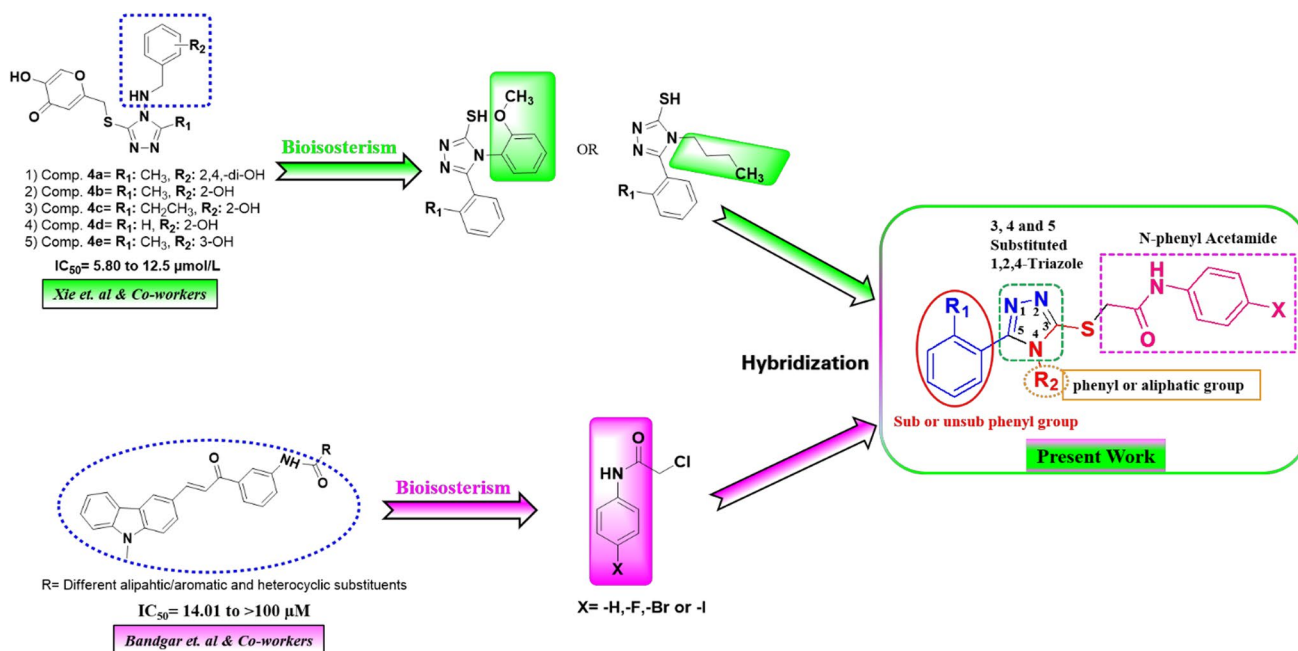
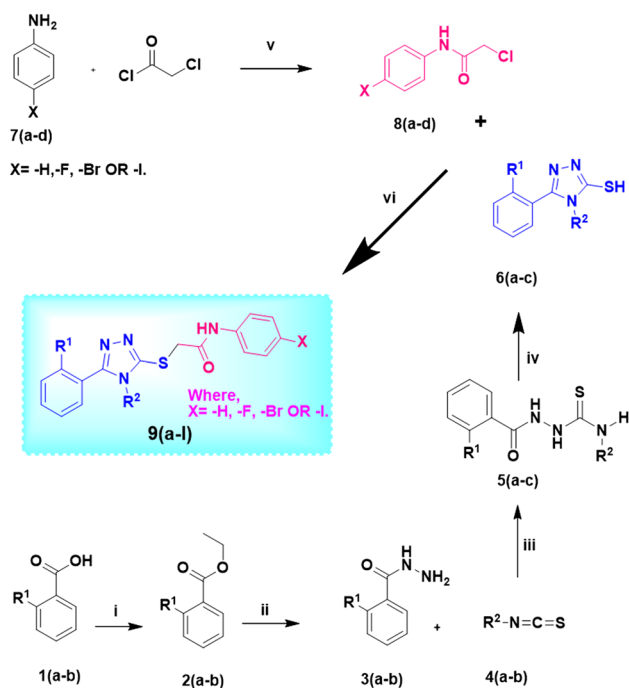


Fig. 1 Fragment-founded strategy of proposed tyrosinase inhibitors



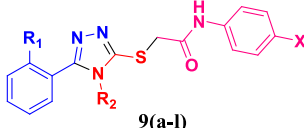
Scheme 1 Synthesis route, reagents and conditions: (i) EtOH, conc. H₂SO₄; (ii) hydrazine hydrate, EtOH, reflux; (iii) ethanol, 12 h, RT; (iv) DM water, 2 N NaOH, 70–80 °C, (v) triethyl amine, MDC; (vi) potassium carbonate, DMF, RT

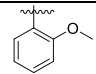
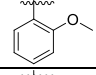
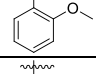
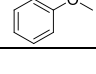
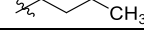
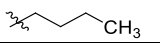
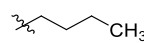
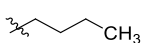
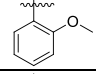
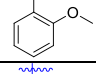
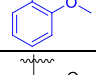
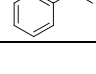
6(a-c). In order to complete the synthesis of the target compound, another key intermediate has been synthesized by the simple coupling of the different sub/

unsubstituted aniline derivatives **7(a-d)** and 2-chloroacetyl chloride (2CAC) in the presence of triethyl amine as a base to form corresponding 2-chloro-*N*-halogen sub/unsubstituted phenyl acetamide derivatives **8(a-d)**. Lastly, the 1,2,4-triazole-3-thiol derivatives **6(a-c)** were coupled with electrophile (benzamide derivatives) **8(a-d)** in existence of a base (K₂CO₃) using DMF as solvent to form a corresponding target compound **9(a-l)** with decent yield. The general representative structure of the target compounds appeared is formulated in Table 1. Furthermore, the progress of the chemical reactions was authenticated by TLC methodology and the manufactured compounds were purified by using column chromatography method. The structural interpretation of the target compounds **9(a-l)** was done by using FTIR, LC-MS, ¹H NMR and ¹³C NMR analytical skills.

In vitro tyrosinase activity and structural activity relationship (SAR)

The novel synthesized triazole-based heterocyclic target compounds **9(a-l)** were screened in contradiction to mushroom tyrosinase enzyme. The gained result reveals that these molecules' IC₅₀ value ranges from 0.0048 ± 0.0016 to 0.6545 ± 0.0988 μM relative to standard inhibitor kojic acid having IC₅₀ value 16.8320 ± 1.1600 μM as presented in Table 1. In practice, the achieved inhibitory activity in a molecule is due to the involvement of the entire molecule but a partial SAR study was streamlined by the presence of the distinct substituents in respective target compounds, in

Table 1 Different substituents present in target compounds and IC₅₀ value for tyrosinase activity


Sr. No	Compound	-R ₁	-R ₂	-X	Tyrosinase activity IC ₅₀ ± SEM (μM)
1	9a	-F		-H	0.5425±0.0715
2	9b	-F		-F	0.1691±0.0086
3	9c	-F		-Br	0.1537±0.0024
4	9d	-F		-I	0.0605±0.0096
5	9e	-H		-H	0.2144±0.0368
6	9f	-H		-F	0.3696±0.2293
7	9g	-H		-Br	0.3431±0.0749
8	9h	-H		-I	0.2179±0.0478
9	9i	-H		-H	0.0238±0.0077
10	9j	-H		-F	0.0802±0.0032
11	9k	-H		-Br	0.0048±0.0016
12	9l	-H		-I	0.6545±0.0988
13	Kojic Acid (Standard)				16.8320±1.1600

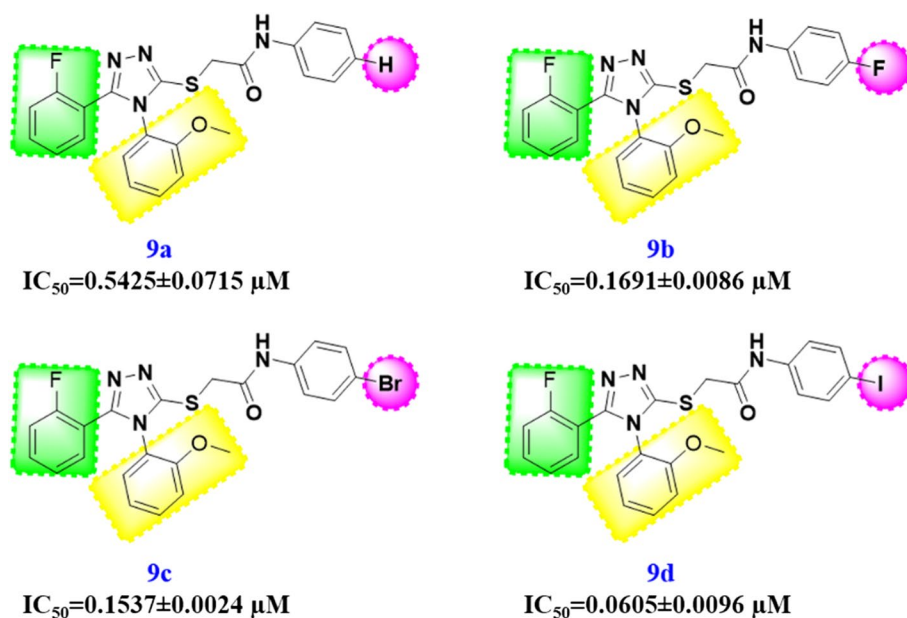
SEM = standard error of the mean; values are expressed in mean ± SEM

which it has more prospects to fluctuate the inhibitory activity of the corresponding target compound because of the presence of the distinct interaction pattern with the enzyme, which was clearly distinguished by SAR study. Furthermore, all the integrated compounds **9(a-l)** possess good activity, but among all of them, compound **9k** exhibits the most effective inhibitory activity against mushroom tyrosinase enzyme.

As displayed in Fig. 2, All the four target compounds **9a**, **9b**, **9c** and **9d** consist of same scaffold (*i.e.* 1,2,4-triazol-3-ylthio)-*N*-phenyl acetamide) but only the change in para-substituents of acetamide group. At this point, the 4- and 5-positions in 1,2,4-triazole scaffold possess an *ortho*-methoxy phenyl group and an *ortho*-fluoro phenyl group, which were unchanged for these four derivatives as indicated

in Fig. 2. In fact, compound **9a** (IC₅₀ = 0.5425 ± 0.0715 μM) does not contain any halogen substituent or contains hydrogen atom at *para* position in acetamide functional group, while the compounds **9b** (IC₅₀ = 0.1691 ± 0.0086 μM), **9c** (IC₅₀ = 0.1537 ± 0.0024 μM) and **9d** (IC₅₀ = 0.0605 ± 0.0096 μM) have fluoro, bromo, and iodo substituents at *para*-position, respectively. As a result, the compound which holds an iodo group possesses a good inhibitory activity. From the *in vitro* study, we observed that the compounds (**9c**, **9d** and **9d**) which cover halogen atoms (-F, -Br and -I) at *para*-position in acetamide functionality display better activity than compound (**9a**) which does not contain halogen substituent at *para*-position. It means that as the size of the halogen atoms increases at the *para*-position in the acetamide functional group, the interaction with

Fig. 2 Structural activity relationship of **9a**, **9b**, **9c** and **9d**

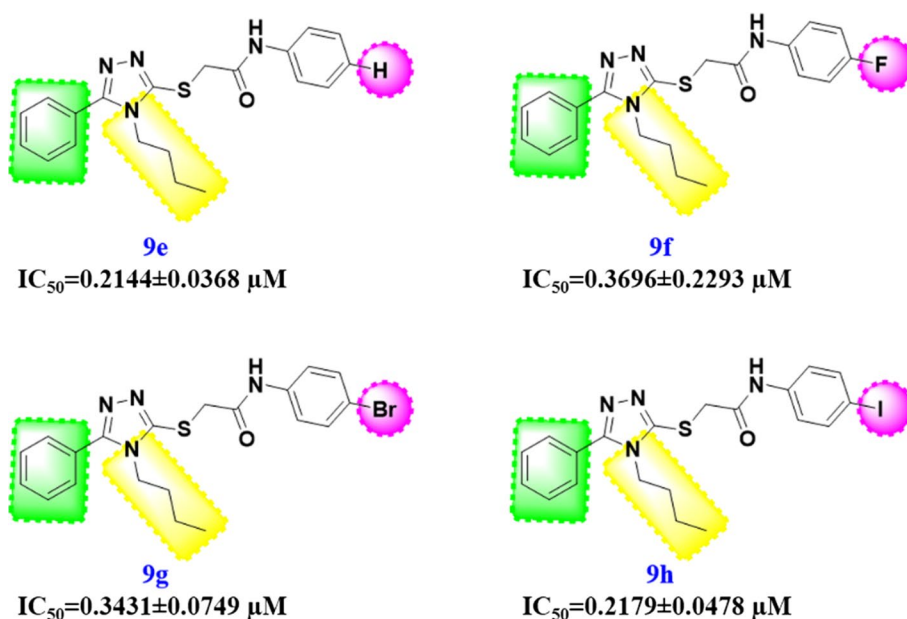


the enzyme becomes more and more powerful, resulting in increased activity trend in the respective triazole derivatives. The isomer can be organized as per the inhibitory activity: **9d** > **9c** > **9b** > **9a**. Therefore, from the SAR study, compound **9d** confirms a good inhibitory activity counter to mushroom tyrosinase enzyme since it contains more heavier halogen (-I) atom at the para-position in the acetamide functionality of the triazole derivatives.

Furthermore, the scaffold was changed at 4 and 5 positions in 1,2,4-triazol-3-ylthio)-*N*-phenyl acetamide. In compounds **9e**, **9f**, **9g** and **9h**, the 4- and 5-positions have been replaced by aliphatic *n*-butyl and aromatic phenyl groups, respectively, which was ordinary for

four derivatives **9(e-h)** but only the substituents ($X = \text{H}$, F , Br or I) are changed at the para-position in acetamide functionality as shown in Fig. 3. Hereby, the compound **9e** ($IC_{50} = 0.2144 \pm 0.0368 \mu\text{M}$) bearing hydrogen, similarly compounds **9f** ($IC_{50} = 0.3696 \pm 0.2293 \mu\text{M}$), **9g** ($IC_{50} = 0.3431 \pm 0.0749 \mu\text{M}$) and **9h** ($IC_{50} = 0.2179 \pm 0.0478 \mu\text{M}$) contain fluoro, bromo and iodo substituents at the para-position in the acetamide functional group. In the case of compounds **9e** and **9h**, carrying hydrogen (-H) and iodo (-I) substituents at the para-position in acetamide functionality demonstrate almost the same interaction with enzyme and exhibit auspicious inhibitory activity against tyrosinase. But in the case of fluoro and bromo

Fig. 3 Structural activity relationship of **9e**, **9f**, **9g** and **9h**



substituents (**9f** and **9g**), the interaction with the enzyme was not much more effective. Additionally, after evaluating the in vitro outcomes of the target derivatives **9(a–d)** with the respective compounds **9(e–h)**, the result indicates that compounds **9(b–d)** confirm superior interaction than the respective compounds **9(f–h)** with exception of nonhalogenated compounds **9a** and **9e**, respectively (Figs. 2, 3).

Also, the compounds **9(a–d)** have been slightly modified by replacing the ortho/fluoro phenyl group to phenyl moiety at 5-position in the 1,2,4-triazole scaffold to offer four new compounds **9i**, **9j**, **9k** and **9l**, respectively, as shown in Fig. 4. Compounds **9i** ($IC_{50}=0.0238\pm 0.0077\ \mu\text{M}$) and **9j** ($IC_{50}=0.0802\pm 0.0032\ \mu\text{M}$) display capable activity, and they contain a hydrogen and fluorine atom at para-position concerning acetamide functional group. But in the case of bromo substitution, it shows an excellent activity among the series as well as compared with standard drug kojic acid ($IC_{50}=16.8320\pm 1.1600\ \mu\text{M}$) but in case of iodo-substituted compounds, i.e., **9l** ($IC_{50}=0.6545\pm 0.0988\ \mu\text{M}$), it exhibits a reverse trend. Additionally, after comparing the IC_{50} values of the **9(i–l)** with the respective compounds **9(a–d)** and **9(e–h)**, it was observed that the target compounds **9d**, **9i**, **9j** and **9k** confirm the most effective interaction among the series, but in the case of iodo-substituted derivatives, they exhibit anomalous comportment.

Finally, from the structural activity relationship (SAR) assessment, it was noticed that the compounds which possess aromatic substituent at 4-position in 1,2,4-triazol-3-ylthio)-*N*-(phenyl) acetamide scaffold demonstrate good inhibition outcome than aliphatic-substituted compound (Figs. 2, 3, 4). Also, the trend was acceptable when the halogens are substituted at para-position with respect to

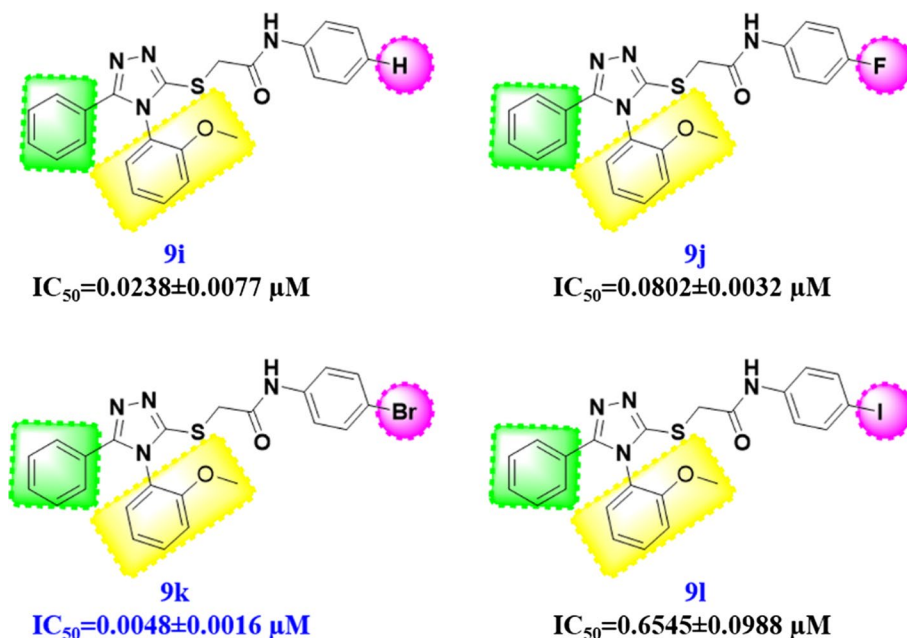
acetamide functionality. But this trend was proved up to bromo substitution; afterward, the irregular behaviour of the iodo compound appears. The synthesized target compounds **9(a–l)** are organized corresponding to their effective interaction pattern achieved as per in vitro report, for instance **9k** > **9i** > **9d** > **9j** > **9c** > **9b** > **9e** > **9h** > **9g** > **9f** > **9a** > **9l** (IC_{50} values are mentioned in Table 1 and Fig. 2, 3, 4).

In vitro analysis

Kinetic analysis

Based on our results, we select the most potent compound **9k** to determine inhibition type and inhibition constant of tyrosinase. The potential of these compounds to inhibit free enzyme and enzyme–substrate complex was determined in terms of EI and ESI constants, respectively. The kinetic studies of the enzyme by the Lineweaver–Burk plot of $1/V$ versus $1/[S]$ in the presence of different compounds concentrations gave a series of straight lines (Fig. 5A). The results of compound **9k** showed that compound intersected within the second quadrant. The analysis showed that V_{max} decreased to new increasing doses of inhibitors and on the other hand K_m remains the same. This behaviour indicates that compound **9k** inhibits the tyrosinase noncompetitively to form the enzyme–inhibitor complex. The secondary plot of slope against the concentration of inhibitors showed enzyme inhibitor dissociation constant (K_i) (Fig. 5B). The kinetic results are presented in Table 2 (kinetic parameter table).

Fig. 4 Structural activity relationship of **9i**, **9j**, **9k** and **9l**



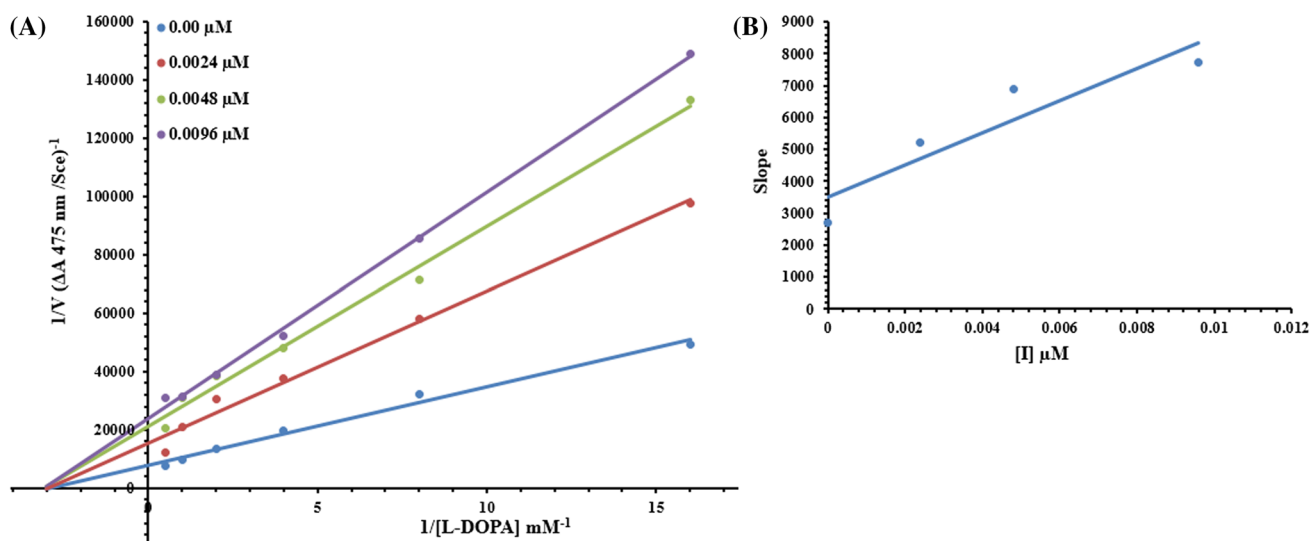


Fig. 5 Lineweaver–Burk plots for inhibition of tyrosinase in the presence of compound **9k**. (A) Concentrations of **9k** were 0.00, 0.0024, 0.0048 and 0.0096 μM , respectively. Substrate L-DOPA concentrations were 0.0625, 0.125, 0.25, 0.5, 1 and 2 mM, respectively. (B)

Table 2 Kinetic parameters of the mushroom tyrosinase for L-DOPA activity in the presence of various concentrations of **9k**

Concentration (μM)	V_{max} ($\Delta A/S$)	K_m (mM)	Inhibition type	K_i (μM)
0.00	0.00013	0.28	Noncompetitive	0.007
0.0024	8.236×10^{-5}	0.28		
0.0048	4.8551×10^{-5}	0.28		
0.0096	3.2204×10^{-5}	0.28		

V_{max} is the reaction velocity, K_m is the Michaelis–Menten constant, K_i is the EI dissociation constant

Cytotoxicity study

There are many skin-lighting compounds available in the market, namely kojic acid, PTU, hydroquinone arbutin, etc., which are being broadly exploited as a skin-whitening agent [43, 44]. But to full fill, the criteria of the potent skin whitening agent should be reliable, without objectionable cytotoxic side effect. Herein, we have synthesized 12 novel triazole founded tyrosinase inhibitors and all proved to have decent activity against mushroom tyrosinase inhibitor compared with standard kojic acid. But among all, we have preferred four extremely potent inhibitors (**9d**, **9i**, **9j** and **9k**) for cytotoxicity experiment. The cell toxicity experiment was carried out by using the MTT assay for A375 human melanoma cells. The cells were cultivated for 24 h at various concentrations (1, 5, 10, 15, 20, and 25 $\mu\text{g/ml}$) of the most potent compounds **9d**, **9i**, **9j** and **9k**, respectively, and the results on cell viability assay are specified in Fig. 6. From the cell viability experiment,

The insets represent the plot of the slope versus inhibitor **9k** concentrations to determine inhibition constant. The lines were drawn using linear least squares fit

all the compounds demonstrate cell viability of approximately 80%, against nontreated cells. Thus, all the potent compounds are not toxic to the A375 human melanoma cells in the concentration scale between 0 and 25 $\mu\text{g/ml}$. Nevertheless, after comparison among the series, the most potent compounds **9d**, **9i**, **9j** and **9k** are proved to have the more acceptable result in cell cytotoxicity experimentation. Hence, the target compound **9k** could be employed as excellent tyrosinase inhibitor in the field of medicinal chemistry for the development of the new drug.

In silico analysis

Binding energy evaluation of the synthesized derivatives

To predict the best-fitted conformational position of synthesized ligands **9(a–l)** within the active region of the target protein, the generated docked complexes were observed based on glide docking energy values (kcal/mol) and bonding interaction (hydrogen/hydrophobic) pattern. The lowest binding energy value depicts the best conformational position of the ligand within the active region of the target protein. The docking results showed that all the synthesized ligands **9(a–l)** were bound within the active site of the target protein with different conformational poses and energy values, respectively (Fig. 7A, B). The comparative results showed that compounds exhibited good docking energy values. The basic skeleton of all the synthesized compounds was similar; therefore, no considerable variation was noticed in docking energy of all synthesized ligands.

Fig. 6 Cell viability measurement using the MTT assay. Cells were untreated (control) or treated with most potent compounds **9d**, **9i**, **9j** and **9k** at different concentrations (1, 5, 10, 15 and 25 $\mu\text{g/ml}$) in DMSO for 24 h

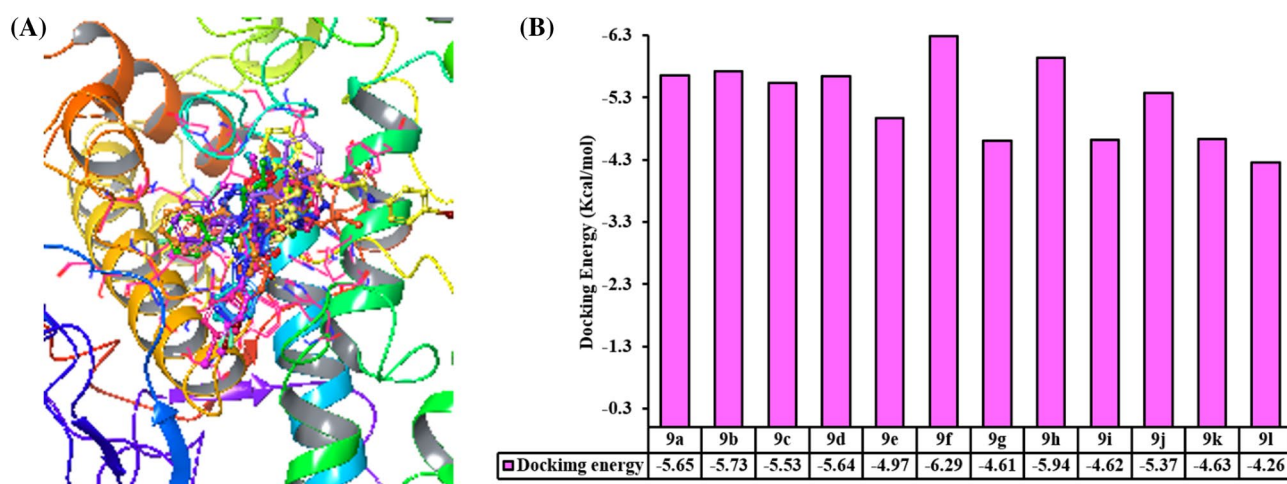
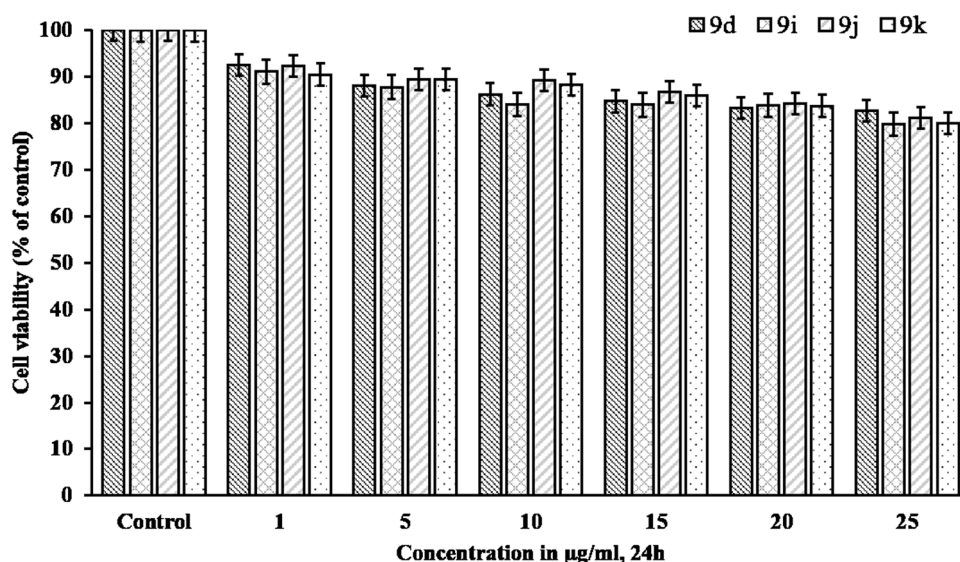


Fig. 7 (A) Docking complex of **9(a-l)** within the active region of target protein. (B) Graphical presentation of docking energy values of complexes **9(a-l)**

Ligand-binding analysis of tyrosinase docked complexes

Based on in vitro results, the **9k** docking complex was selected to check the binding conformational analysis. In detailed docking analysis, couple of hydrogen bonds and three π - π interactions were observed in the best potent ligand docking complex. The carbonyl oxygen atom of **9k** formed two hydrogen bonds with Arg268 with a bonding distance of 2.20 Å (Fig. 8A). Moreover, phenyl ring of 4-bromobenzene and another phenyl ring substituted at 3-position in 1,2,4-triazole core of **9k** formed two π - π interactions with Phe264. Similarly, the 1,2,4-triazole ring also interacted with the same residue Phe264 through π - π interaction. The hydrogen and π - π bonds gave more stability to **9k** within the active region of the target protein.

The binding pocket analysis depicted that **9k** showed good binding conformation within binding pocket residues. The 2D graphical depiction of the docking complex is done in Fig. 8B. Literature data also ensured the importance of these residues in bonding with other tyrosinase inhibitors which strengthen our docking results [45–48].

Molecular dynamic simulations (MDS)

Root-mean-square deviation and fluctuation (RMSD/RMSF) To evaluate the residual flexibility of receptor through MD simulation, RMSD and RMSF graphs were evaluated to determine the protein structural behaviour. The RMSD is used to measure the average change in displacement of a selection of atoms for a frame with respect to a

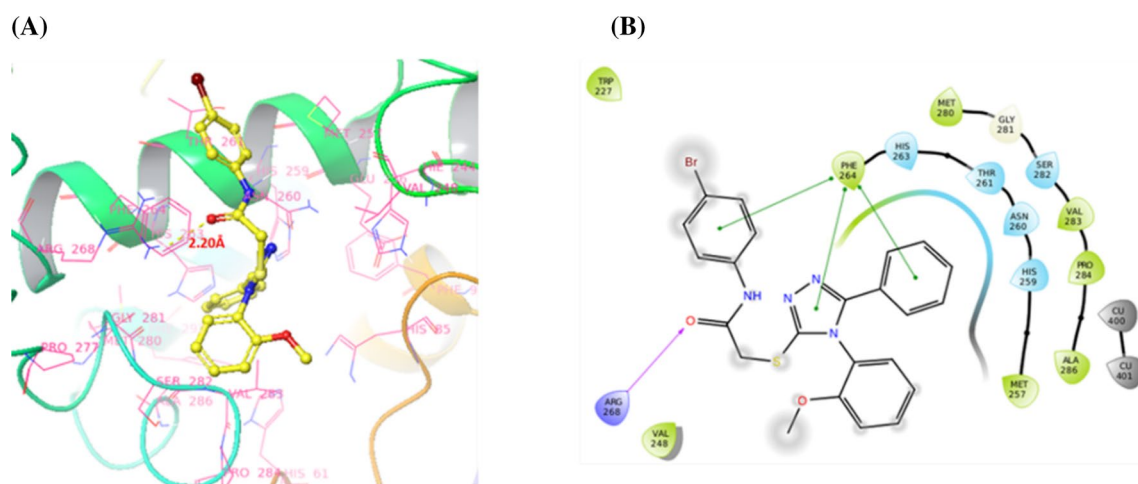


Fig. 8 (A) 3D docking depiction of **9k** complex against tyrosinase. (B) 2D docking depiction of **9k** complex against tyrosinase

reference frame. The RMSD graph result of **9k** interprets the protein residual deviation in 100 ns simulation time frame. Initially, the graph lines showed an increasing trend from 0 to 20 ns having RMSD value range from 1.2 to 2.4 Å for C α , backbone and side chains, respectively. From 20 to 60 ns, C α and backbone graph lines remain stable and no high fluctuations were observed and RMSD values remained the same. Moreover, after 60 ns, a little increasing fluctuation was observed and RMSD values for C α , backbone and side chains rose to 1.6 and 2.8 Å, respectively. Furthermore, from 60 to 100 ns, all graph lines remained steady stable and no high fluctuations were observed. The overall RMSD analysis showed that fluctuations of all graphs in the whole simulation are within the standard range of RMSD 1–3 Å (Fig. 9). The RMSF is useful for characterizing local changes along with the protein structure. The generated plot indicated protein behaviour fluctuations during the simulation in C α residues. The overall results showed that the tails N-and C-terminals little fluctuated expect the residues

around 250 amino acids. Secondary structure elements such as alpha helices and beta strands are usually more rigid than the unstructured part of the protein and thus fluctuated less than the loop regions (Fig. 10).

Protein interactions with the ligand can be monitored throughout the simulation. It has been obtained that protein–ligand interactions are categorized into four types: (1) hydrogen bonds, (2) hydrophobic, (3) ionic and (4) water bridges. The generated stacked bar charts showed that a couple of residues Phe264 and Trp227 have interacted with the ligand. The interaction fractions for both residues were higher than 0.7, which suggested that 70% of the simulation time is specifically maintained in interaction behaviour (Fig. 11).

Fig. 9 RMSD graph of **9k** docking complex at 100 ns

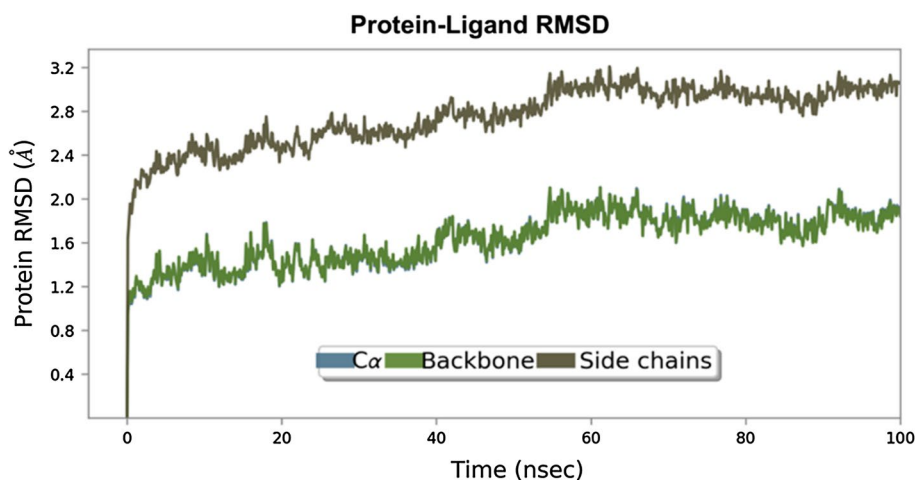


Fig. 10 RMSF graph of **9k** docking complex at 100 ns

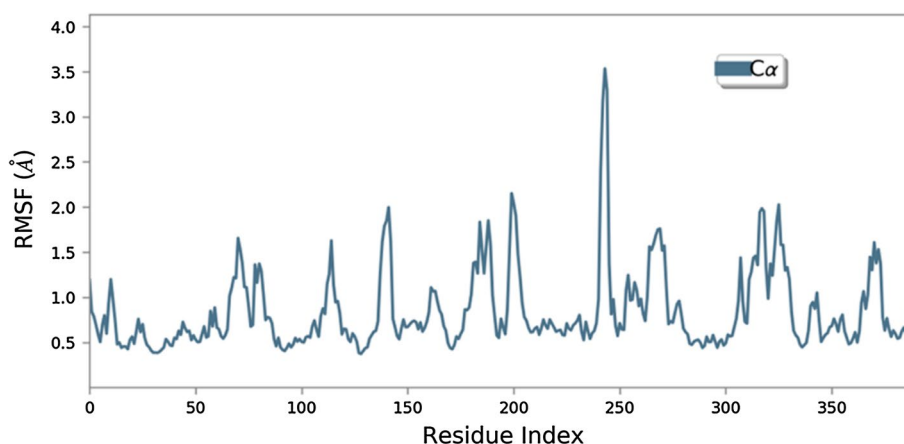
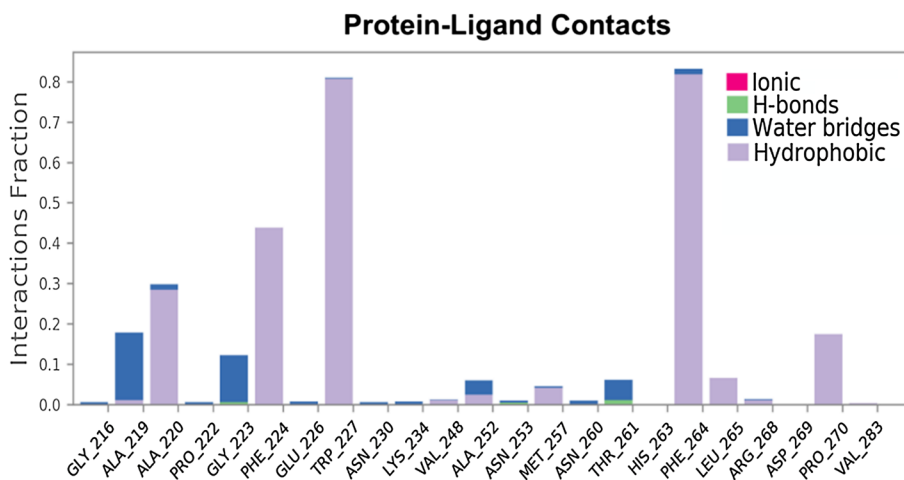


Fig. 11 Protein–ligand contacts of **9k** docking complex



Conclusion

In summary, we have defined the successful synthesis of the 1,2,4-triazole derivatives via a multistep pathway under simplistic conditions and these 12 novel target compounds were achieved with good yields. The synthesized target derivatives were well substantiated through spectral data analysis of FTIR, LCMC, ^1H & ^{13}C NMR; and investigated for their in vitro study, counter to mushroom tyrosinase inhibition. From the in vitro study, it was observed that all the synthesized target compounds **9(a–l)** exhibit decent activity against mushroom tyrosinase enzyme compared with reference kojic acid. Besides, among all the derivatives, compounds **9k** ($\text{IC}_{50} = 0.0048 \pm 0.0016 \mu\text{M}$) are almost 3500-fold more active with the aggressive mechanism of action than standard drug kojic acid ($\text{IC}_{50} = 16.8320 \pm 1.1600 \mu\text{M}$). Also, to validate the non-toxic actions of the most potent compounds, has been proven by using the cytotoxicity experiment, which was carried out using MTT assay method for A375 human melanoma cells. Cell viability of the most potent compounds

(**9d**, **9i**, **9j**, **9k**) has been calculated at various concentrations ranging from 0 to 25 $\mu\text{g}/\text{ml}$. The results reveal that all the potent compounds confirm nontoxic performance against A375 human melanoma cells even treated at high concentrations. Furthermore, the docking assessment was conducted to analyse the binding contact of the ligand with an enzyme. Besides, the simulation experiment gives us an idea about the binding pattern of the ligand with an enzyme, which shows that residues Phe264 and Trp227 more effectively interacted with a ligand. Overall, it can be assumed from the experiment that the synthesized target compound **9k** could be used as a good candidate of the drug in a pharmaceutical field for the development of the new drug.

Materials and methods

Chemistry

The chemicals required for the synthesis of the target compounds were bought from Sigma-Aldrich (Munich,

Germany) and Samchun Chemicals (Daejeon, South Korea) and used without purification. ^{13}C NMR and ^1H NMR spectra were taken in DMSO- d_6 using a Bruker Avance (Germany) NMR spectrophotometer at 101 and 400 MHz, respectively. The mass analysis (LC-MS) was performed on 2795/ZQ2000 (waters) spectrometer. The IR spectra were filmed on Frontier IR spectrophotometer (Perkin Elmer, USA). The improvement in the reactions was monitored by a thin-layer chromatography (TLC) technique. The physical parameters (such as melting points) of the compounds (**9a–9l**) were determined by using Fisher Scientific (USA) melting point tool and are uncorrected. The coupling constant and chemical shift values are mentioned in ppm and Hz, respectively.

General synthetic procedure for the key intermediates (**2a–2g**) and (**3a–3b**)

The intermediates **2(a–b)** and **3(a–b)** were prepared by following previously reported method [49, 50].

General synthetic procedure for the key intermediate **5(a–c)**

The respective hydrazide intermediate compound, i.e., **3(a–b)** (1 mmol) in ethanol (2 mL), was added to a RBF at room temperature under atmospheric nitrogen and it was continued to be stirred for an additional 10–15 min, and then corresponding isothiocyanate compound **4(a–b)** (1 mmol) was added under nitrogen environment. The reaction was continued till the accomplishment of the reaction (10–12 h). The formation of the product was verified by TLC system. The precipitated solid was filtered and washed with cold ethanol and then dried to afford an open-ring intermediate **5(a–c)** with good yield and utilized as such for the next step.

General synthetic procedure for the key intermediate **6(a–c)**

As shown in Scheme 1, the different intermediate compounds **5(a–c)** (1 mmol) were taken in distilled water and heated to 35–40 °C for 10 min and then 2 N NaOH (pH of reaction mixture > 10) solution was added to it, and then the mixture was heated for 4–5 h at 70–80 °C. Product confirmation was checked by TLC technique. Afterward, the reaction mass was slowly cooled down to RT (room temperature) and distilled water was added and then it was cooled to 0–5 °C. The pH (5–6) of the reaction mass was adjusted by adding 2 N HCl solution (Conc. HCl was used wherever necessary). After maintaining the pH, the reaction mass was continued to be stirred for 1–2 h at 10–15 °C, and then the solid was filtered and dried to afford a compound **6(a–c)**, which was taken as it is for the next step.

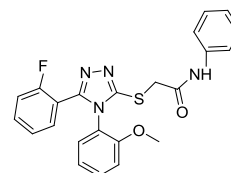
General synthetic procedure synthesis for the key intermediate **8(a–d)**

As stated in Scheme 1, the respective aniline compound **7(a–d)** (1 mmol) was taken in dichloromethane (MDC) and chilled to 0 °C. Subsequently, triethyl amine (1.2 mmol) was added to the precooled reaction mass and stirred for 15–20 min. Meanwhile, in another flask, a solution of 2-Chloroacetyl chloride (2-CAC) (1 mmol) was taken in MDC under atmospheric nitrogen condition and cooled to 0 °C. The above precooled reaction mass of respective aniline and triethyl amine was gradually added to the 2-CAC reaction mass at 0 °C (evolution of HCl gas). After completion of the addition, the reaction mixture was continued to be stirred for another 2 h, and then the temperature was steadily raised to RT and retained for an additional 1–2 h. The reaction improvement was noticed by TLC. After the achievement of the reaction, distilled water was added to the reaction mixture, which was then quenched with water and extracted with MDC. The MDC layer was concentrated, and crude residue was purified by using column chromatography technique eluting with hexane/ethyl acetate (1–10%) as a solvent to afford a pure compound **8(a–d)**, which was used for the synthesis of the objective compounds **9(a–l)**.

General procedure for the synthesis of the target compounds **9(a–l)**

As displayed in Scheme 1, an intermediate compound **6(a–c)** (1 mmol) and potassium carbonate were taken in dimethylformamide (DMF) and stirred at RT for 15–20 min. Subsequently, intermediate compound **8(a–d)** (1 mmol) was added and continued to be stirred for 4–5 h, until the completion of the reaction (reaction enhancement supported via TLC approach). The reaction accomplishment was analysed by TLC. Later, distilled coldwater was added to the reaction mass and stirred for 20 min (solid was obtained). The acquired solid was filtered, washed several times with distilled cold water and suck dried. Further, the solid was dried and purified by using column chromatography technique eluting with the hexane and ethyl acetate as a solvent to afford a pure 1,2,4-triazole derivatives **9(a–l)** with good yield.

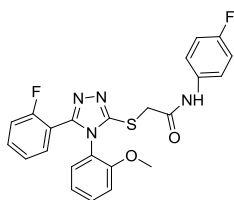
2-(5-(2-Fluorophenyl)-4-(2-methoxyphenyl)-4H-1,2,4-triazol-3-ylthio)-N-phenylacetamide (**9a**)



White solid; isolated

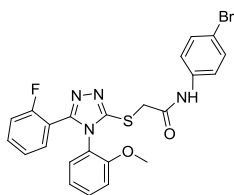
yield: 80%; M.P: 154 °C; (ESI, Fig. S1): ^1H NMR data: δ H (400 MHz, DMSO- d_6) 10.37 (1 H, s), 7.58 (2 H, d, $J=7.6$), 7.52–7.44 (2 H, m), 7.41 (1 H, dd, $J=7.7, 1.8$), 7.37–7.30 (3 H, m), 7.26–7.18 (2 H, m), 7.16 (1 H, dd, $J=8.4, 0.9$), 7.08 (1 H, t, $J=7.4$), 7.05–6.99 (1 H, m), 4.24 (1 H, d, $J=15.0$), 4.20 (1 H, d, $J=15.0$), 3.62 (3 H, s); (ESI, Fig. S2): ^{13}C NMR (101 MHz, DMSO- d_6) δ 165.98, 154.41, 132.27, 131.90, 129.29, 129.08, 124.01, 121.28, 119.59, 116.44, 113.35, 56.22, 37.39; (ESI, Fig. S3): IR (KBr): 3250, 3193, 3131, 3093, 2933, 2845, 1678, 1622, 1177, 1094, 820 and 687 cm^{-1} ; (ESI, Fig. S4): LC–MS: 435.2 (m/z).

N-(4-fluorophenyl)-2-(5-(2-fluorophenyl)-4-(2-methoxyphenyl)-4H-1,2,4-triazol-3-ylthio) acetamide (9b)



Light-grey solid; isolated yield: 82%; M.P: 105 °C; (ESI, Fig. S5): ^1H NMR (400 MHz, DMSO- d_6) δ 10.48 (s, 1H), 7.96 (s, 1H), 7.67–7.55 (m, 2H), 7.52–7.37 (m, 3H), 7.34 (dd, $J=7.8, 1.5$ Hz, 1H), 7.28–7.10 (m, 4H), 7.03 (ddd, $J=7.7, 1.0$ Hz, 1H), 4.20 (s, 2H), 3.62 (s, 3H); (ESI, Fig. S6): ^{13}C NMR (101 MHz, DMSO- d_6) δ 162.78, 132.27, 131.89, 129.08, 121.42, 121.34, 121.27, 115.97, 115.74, 113.35, 56.22, 52.62, 36.25; (ESI, Fig. S7): IR (KBr): 3251, 3192, 3132, 3038, 2933, 2845, 1679, 1622, 1177, 1163, 1094, 751 and 687 cm^{-1} ; (ESI, Fig. S8): LC–MS: 453.2 (m/z).

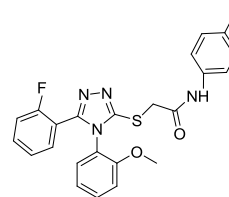
N-(4-bromophenyl)-2-(5-(2-fluorophenyl)-4-(2-methoxyphenyl)-4H-1,2,4-triazol-3-ylthio) acetamide (9c)



Dark-grey solid; isolated yield: 82.5%; M.P: 112 °C; (ESI, Fig. S9): ^1H NMR δ H (400 MHz, DMSO- d_6) 10.54 (1 H, s), 7.60–7.54 (2 H, m), 7.50 (3 H, ddd, $J=8.0, 7.3, 4.1$), 7.47–7.44 (1 H, m), 7.41 (1 H, td, $J=7.6, 1.8$), 7.34 (1 H, dd, $J=7.8, 1.5$), 7.22 (2 H, ddd, $J=8.7, 6.8, 3.3$), 7.18–7.13 (1 H, m), 7.03 (1 H, td, $J=7.7, 1.0$), 4.26–4.16 (2 H, s), 3.62 (3 H, s); (ESI, Fig. S10): ^{13}C NMR (101 MHz, DMSO- d_6) δ 132.28, 132.12, 131.89, 129.07, 127.20, 124.99, 121.53, 121.28, 115.59, 113.36, 56.23, 52.63, 37.34; (ESI, Fig. S11): IR (KBr): 3250, 3193, 3132, 3071.85, 3038.88, 2933.32,

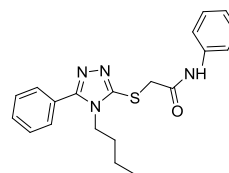
2845.47, 1678.69, 1622.18, 1177.60, 1163.22, 1021.20, 1001.91, 750.88 and 987.54 cm^{-1} ; (ESI, Fig. S12): LC–MS: 515.1 (m/z).

2-(5-(2-fluorophenyl)-4-(2-methoxyphenyl)-4H-1,2,4-triazol-3-ylthio)-N-(4-iodophenyl) acetamide (9d)



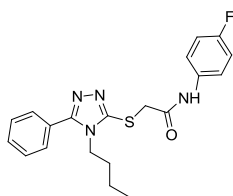
Brown solid; isolated yield: 85%; M.P: 220 °C; (ESI, Fig. S13): ^1H NMR (400 MHz, DMSO- d_6) δ 10.48 (s, 1H), 7.69–7.65 (m, 2H), 7.52–7.38 (m, 5H), 7.34 (dd, $J=7.8, 1.5$ Hz, 1H), 7.28–7.11 (m, 3H), 7.03 (dd, $J=7.6, 1.1$ Hz, 1H), 4.23 (d, $J=15.1$ Hz, 1H), 4.18 (d, $J=15.1$ Hz, 1H), 3.62 (s, 3H); (ESI, Fig. S14): ^{13}C NMR (101 MHz, DMSO- d_6) δ 166.20, 139.10, 137.95, 132.23, 131.90, 129.07, 121.78, 121.28, 116.44, 116.23, 113.36, 56.22 and 37.37; (ESI, Fig. S15): IR (KBr): 3250.82, 3192.87, 3133.61, 3071.26, 3038.34, 2923.51, 2849.77, 1678.72, 1622.14, 1177.65, 1024.75, 750.92 and 687.70 cm^{-1} ; (ESI, Fig. S16): LC–MS: 561.1 (m/z).

2-(4-butyl-5-phenyl-4H-1,2,4-triazol-3-ylthio)-N-phenyl acetamide (9e)



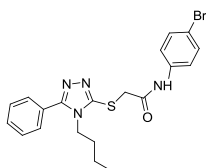
White solid; isolated yield: 82%; M.P: 103 °C; (ESI, Fig. S17): ^1H NMR (400 MHz, DMSO- d_6) δ 10.40 (s, 1H), 7.65–7.61 (m, 2H), 7.61–7.54 (m, 5H), 7.36–7.28 (m, 2H), 4.21 (s, 1H), 4.02 (t, 2H), 1.54 (qui, 2H), 1.13 (sxt, 2H), 0.74 (t, $J=7.4$ Hz, 3H); (ESI, Fig. S18): ^{13}C NMR (101 MHz, DMSO- d_6) δ 166.16, 155.56, 139.29, 130.52, 129.46, 129.28, 128.91, 127.83, 124.01, 119.59, 52.62, 44.45, 38.15, 29.51, 29.16, 22.55, 19.43, 14.42; (ESI, Fig. S19): IR (KBr): 3249.97, 3192.64, 3132.27, 3018.51, 2921.02, 2850.87, 1679.01, 1622.07, 1177.86, 1094.37, 751.52 and 687.81 cm^{-1} ; (ESI, Fig. S20): LC–MS: 367.2 (m/z).

2-(4-butyl-5-phenyl-4H-1,2,4-triazol-3-ylthio)-N-(4-fluorophenyl) acetamide



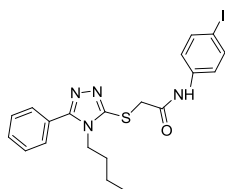
(9f) Off-white solid; isolated yield: 81%; M.P: 108 °C; (**ESI**, Fig. S21): ^1H NMR (400 MHz, DMSO-d_6) δ 10.45 (s, 1H), 7.66–7.53 (m, 7H), 7.21–7.13 (m, 2H), 4.20 (s, 2H), 4.06–3.97 (m, 2H), 1.54 (qui, 2H), 1.13 (Sxt, $J=14.6$, 7.3 Hz, 3H), 0.74 (t, $J=7.4$ Hz, 3H); (**ESI**, Fig. S22): ^{13}C NMR (101 MHz, DMSO) δ 166.09, 155.56, 150.49, 135.69, 130.53, 129.46, 128.91, 127.82, 121.41, 121.33, 115.98, 115.76, 52.63, 44.45, 38.01, 31.75, 31.64, 29.51, 19.43, 13.60; (**ESI**, Fig. S23): IR (KBr): 3252, 3194, 3023, 2922, 2851, 1679, 1601, 1178, 1095, 752 and 688 cm^{-1} ; **Fig.** (**ESI**, Fig. S24): LC–MS: 385.2 (m/z).

N-(4-bromophenyl)-2-(4-butyl-5-phenyl-4H-1,2,4-tria-



zol-3-ylthio)acetamide (9g) Grey solid; isolated yield: 79%; M.P: 104 °C; (**ESI**, Fig. S25): ^1H NMR (400 MHz, DMSO-d_6) δ 10.53 (s, 1H), 7.62 (dd, $J=10.4$, 3.3 Hz, 2H), 7.59–7.55 (m, 5H), 7.53–7.49 (m, 2H), 4.21 (s, 2H), 4.04–3.98 (m, 2H), 1.53 (qui, $J=14.9$, 7.5 Hz, 2H), 1.12 (Sxt, $J=14.6$, 7.4 Hz, 2H), 0.74 (t, $J=7.4$ Hz, 3H); (**ESI**, Fig. S26): ^{13}C NMR (101 MHz, DMSO) δ 166.38, 155.57, 150.45, 138.66, 132.13, 130.53, 129.46, 128.91, 127.80, 121.51, 115.61, 52.63, 44.45, 38.06, 31.63, 29.51, 19.43, 13.60; (**ESI**, Fig. S27): IR (KBr): 3249.99, 3192.92, 3038.00, 2919.51, 2850.81, 1679.87, 1622.02, 1177.82, 1094.36, 752.19 and 687.89 cm^{-1} ; (**ESI**, Fig. S28): LC–MS: 447.1 (m/z).

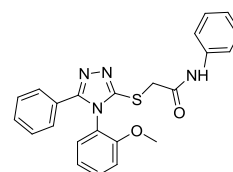
2-(4-butyl-5-phenyl-4H-1,2,4-triazol-3-ylthio)-N-(4-iodophe-



nyl)acetamide (9h) Dark-brown solid; isolated yield: 78%; M.P: 90 °C; (**ESI**, Fig. S29): ^1H NMR (400 MHz, DMSO-d_6) δ 10.48 (s, 1H), 7.70–7.64 (m, 2H), 7.64–7.59 (m, 2H), 7.59–7.54 (m, 3H), 7.46–7.40 (m, 2H), 4.20 (s, 2H), 4.01 (t,

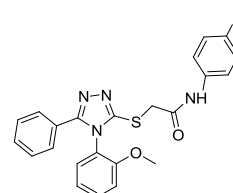
2H), 1.53 (qui, 2H), 1.13 (Sxt, 2H), 0.74 (t, $J=7.4$ Hz, 3H); (**ESI**, Fig. S30): ^{13}C NMR (101 MHz, DMSO) δ 166.37, 155.57, 150.47, 139.11, 137.96, 130.54, 129.46, 128.92, 127.79, 121.76, 87.54, 44.45, 38.09, 31.63, 19.43, 13.60. (**ESI**, Fig. S31): IR (KBr): 3250.76, 3192.30, 3039.34, 2922.09, 2851.49, 2249.80, 1679.29, 1622.49, 1550.55, 1177.99, 1094.61, 820.53, 752.45 and 688.24 cm^{-1} ; (**ESI**, Fig. S32): LC–MS: 493.1 (m/z).

2-(4-(2-methoxyphenyl)-5-phenyl-4H-1,2,4-tria-

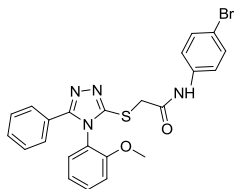


zol-3-ylthio)-N-phenylacetamide (9i) White solid; isolated yield: 82%; M.P: 173 °C; (**ESI**, Fig. S33): ^1H NMR (400 MHz, DMSO-d_6) δ 10.37 (s, 1H), 7.56 (dd, $J=13.3$, 4.8 Hz, 3H), 7.46–7.41 (m, 1H), 7.39–7.30 (m, 7H), 7.27 (d, $J=8.3$ Hz, 1H), 7.09 (dt, $J=12.6$, 7.5 Hz, 2H), 4.21 (d, $J=15.0$ Hz, 1H), 4.17 (d, $J=15.0$ Hz, 1H), 3.66 (s, 3H); (**ESI**, Fig. S34): ^{13}C NMR (101 MHz, DMSO-d_6) δ 166.01, 155.15, 154.84, 139.27, 132.57, 130.23, 129.61, 127.55, 127.35, 124.00, 122.54, 121.70, 119.58, 113.71, 56.43, 37.34; (**ESI**, Fig. S35): IR (KBr): 3250, 3192, 3132, 2923, 2851, 2294, 1678, 1622, 1177 and 820 cm^{-1} ; (**ESI**, Fig. S36): LC–MS: 417.2 (m/z).

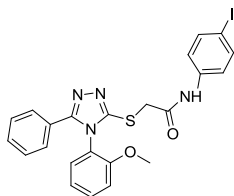
N-(4-fluorophenyl)-2-(4-(2-methoxyphenyl)-5-phe-



nyl-4H-1,2,4-triazol-3-ylthio)acetamide (9j) Off-white solid; isolated yield: 82%; M.P: 88 °C; (**ESI**, Fig. S37): ^1H NMR (400 MHz, DMSO-d_6) δ 10.43 (s, 1H), 7.64–7.54 (m, 3H), 7.43 (dd, $J=7.8$, 1.6 Hz, 1H), 7.40–7.31 (m, 5H), 7.26 (d, $J=7.7$ Hz, 1H), 7.21–7.14 (m, 2H), 7.11 (td, $J=7.7$, 1.0 Hz, 1H), 4.20 (d, $J=15.0$ Hz, 1H), 4.15 (d, $J=15.0$ Hz, 1H), 3.65 (s, 3H); (**ESI**, Fig. S38): ^{13}C NMR (101 MHz, DMSO-d_6) δ 165.95, 155.17, 154.84, 152.36, 135.67, 132.57, 130.24, 129.60, 127.55, 127.35, 122.53, 121.70, 115.98, 113.71, 56.43, 37.22; (**ESI**, Fig. S39): IR (KBr): 3250.25, 3132.75, 3038.62, 2922.42, 2851.51, 1678.71, 1678.71, 1622.19, 1177.81, 1094.38, 752.53 and 688.17 cm^{-1} ; (**ESI**, Fig. S40): LC–MS: 435.1 (m/z).

N-(4-bromophenyl)-2-(4-(2-methoxyphenyl)-5-phenyl-4H

-1,2,4-triazol-3-ylthio) acetamide (9k) Light-grey solid; isolated yield: 84%; M.P: 98 °C; (ESI, Fig. S41): ^1H NMR (400 MHz, DMSO-d_6) δ 10.51 (s, 1H), 7.59–7.54 (m, 3H), 7.53–7.50 (m, 2H), 7.43 (dd, $J=7.8, 1.7$ Hz, 1H), 7.41–7.34 (m, 5H), 7.26 (dd, $J=8.4, 1.0$ Hz, 1H), 7.10 (td, $J=7.6, 1.1$ Hz, 1H), 4.20 (d, $J=15.1$ Hz, 1H), 4.16 (d, $J=15.1$ Hz, 1H), 3.65 (s, 3H); (ESI, Fig. S42): ^{13}C NMR (101 MHz, DMSO-d_6) δ 166.24, 155.17, 154.82, 138.64, 132.58, 132.12, 130.24, 129.60, 129.07, 127.55, 122.45, 121.51, 113.72, 56.43, 37.28; (ESI, Fig. S43): IR (KBr): 3193.01, 3038.63, 2925.19, 2852.90, 2300.62, 2050.74, 1678.54, 1601.77, 1178.78, 1163.21, 1021.71, 764.19 and 688.97 cm^{-1} ; (ESI, Fig. S44): LC–MS: 495.1 (m/z).

N-(4-iodophenyl)-2-(4-(2-methoxyphenyl)-5-phenyl-4H

-1,2,4-triazol-3-ylthio) acetamide (9l) Dark grey solid; isolated yield: 87%; M.P: 203 °C; (ESI, Fig. S45): ^1H NMR (400 MHz, DMSO-d_6) δ 10.47 (s, 1H), 7.70–7.64 (m, 2H), 7.61–7.52 (m, 1H), 7.46–7.33 (m, 8H), 7.26 (dd, $J=8.4, 1.0$ Hz, 1H), 7.10 (td, $J=7.6, 1.1$ Hz, 1H), 4.20 (d, $J=15.1$ Hz, 1H), 4.15 (d, $J=15.1$ Hz, 1H), 3.65 (s, 3H); (ESI, Fig. S46): ^{13}C NMR (101 MHz, DMSO-d_6) δ 166.24, 154.83, 139.10, 137.95, 132.58, 130.24, 129.60, 129.07, 127.55, 122.50, 121.77, 113.71, 56.43, 37.31; (ESI, Fig. S47): IR (KBr): 3193.15, 3038.30, 2923.53, 2852.20, 2300.28, 1678.70, 1601.50, 1244.19, 1178.52, 1021.54, 757.85 and 688.96 cm^{-1} ; (ESI, Fig. S48): LC–MS: 543.1 (m/z).

Biology**In vitro methodology**

In vitro tyrosinase assay The inhibition of mushroom tyrosinase was determined by a modification of the dopachrome method using L-DOPA as a substrate [51–53]. In a detail, 140 μL of phosphate buffer (20 mM, pH 6.8), 20 μL of

mushroom tyrosinase (30 U/mL) and 20 μL of the inhibitor solution were placed in the wells of a 96-well microplate. After pre-incubation for 10 min at room temperature, 20 μL of L-DOPA (3,4-dihydroxyphenylalanine, Sigma Chemical, USA) (0.85 mM) was added and the assay plate was further incubated at 25 °C for 20 min. After the incubation time, the absorbance was measured at 475 nm and the inhibition percentage was calculated concerning the control. Phosphate buffer and kojic acid were tested under the same conditions as the negative and positive controls, respectively. The amount of inhibition by the test compounds was expressed as the percentage of concentration necessary to achieve 50% inhibition (IC_{50}). Each concentration was analysed in three independent experiments. IC_{50} values were calculated by nonlinear regression using GraphPad Prism 5.0.

The % Inhibition of tyrosinase was calculated as follows:

$$\text{Inhibition (\%)} = \frac{[B - S]}{B} \times 100$$

Here, the B and S are the absorbances for the blank and samples.

In vitro kinetic analysis Based on IC_{50} value, we select the most potent compound **9k** for kinetic study. A series of experiments were performed to determine the inhibition kinetics of **9k** by following the already reported methods [43, 54, 55]. The inhibitor concentrations for **9k** were 0.00, 0.0024, 0.0048 and 0.0096 μM . The substrate (L-DOPA) concentrations were between 0.0625 to 2 mM in all kinetic studies. Pre-incubation and measurement time were the same as discussed in the mushroom tyrosinase inhibition assay protocol. Maximal initial velocity was determined from the initial linear portion of absorbance up to 5 min after the addition of enzyme at 30-s interval. The inhibition type of the enzyme was assayed by Lineweaver–Burk plots of the inverse of velocities ($1/V$) versus the inverse of substrate concentration $1/[\text{L-DOPA}] \text{ mM}^{-1}$. The EI dissociation constant K_i was determined by the secondary plot of $1/V$ versus inhibitor concentrations.

Cytotoxicity

Cell culture and treatment of 9d, 9i, 9j and 9k Human malignant melanoma A375 cells were procured from Korean Cell Line Bank (KCLB no.80003, Seoul, Korea). The cells were developed in Dulbecco's altered Eagle's medium (DMEM, Gibco/Invitrogen, Carlsbad, CA, USA) containing 10% foetal bovine serum (FBS, Gibco/Invitrogen) in an incubator with 37 °C, 5% CO_2 and 95% air.

Cell proliferation assay Cells were seeded into 96-well plates with 0.4×10^5 cells/well in 100 μL medium and cul-

tured for 24 h. Following an overnight incubation, the cell medium was removed, and the cells were treated with **9d**, **9i**, **9j** and **9k** concentration gradients (1, 5, 10, 15, 20, and 25 µg/ml) for 24 h. Each treatment included three duplicate wells. The cells with DMSO were used as negative control. The medium was removed, and 0.5 mg/ml 3-(4,5-dimethylthiazol-2-yl)-2,5-diphenyltetrazolium bromide (MTT) was added to each well and incubated for 6 h at 37 °C in an incubator. The medium was removed, and 100 µL solubilization buffer (10% SDS, 0.01 N HCl) was added to each well to terminate the MTT reaction. The plate was covered with foil and agitated on orbital shaker for 1 h to dissolve formazan crystals for the determination of formazan crystal amount, which was measured by the absorbance at 595 nm using a microplate reader (Molecular Devices, Sunnyvale, CA, USA).

Statistical analysis Values are presented as a mean of three different experiments \pm standard deviation (SD). Differences between the calculated means of each individual group were evaluated using a one-way ANOVA.

Docking

Retrieval of mushroom tyrosinase structure from PDB

The three-dimensional (3D) crystal structure of mushroom tyrosinase (*Agaricus bisporus*) (PDBID: 2Y9X) was accessed from the Protein Data Bank (PDB) (<http://www.rcsb.org>). The selected protein was energy minimized by employing conjugate gradient algorithm and amber force field in UCSF Chimera 1.10.1 [56].

Grid generation and molecular docking

Prior to molecular docking, the optimized tyrosinase structure was prepared using the “Protein Preparation Wizard” by Maestro interface in Schrödinger Suite. Bond orders were assigned, and hydrogen atoms were added to the protein. The structure was then minimized to reach the converged root-mean-square deviation (RMSD) of 0.30 Å with the OPLS_2005 force field. The active site of the enzyme is defined from the co-crystallized ligands from Protein Data Bank and literature data [57–59]. The synthesized ligands **9(a–l)** were sketched in s2D sketcher in Schrödinger Suite and saved in Maestro for docking experiment. Furthermore, the docking experiment was performed against all synthesized ligands **9(a–l)** and target protein by using the Glide docking protocol [60]. The predicted binding energies (docking scores) and conformational positions of ligands within the active region of protein were also performed using Glide experiment. Throughout the docking simulations, both partial flexibility and full flexibility around the active site

residues were performed by Glide/SP/XP and induced fit docking (IFD) approaches [61].

Molecular dynamics

The molecular dynamics simulation experiment was carried out using the Desmond simulation package of Schrödinger [62]. In all runs, the NPT (isothermal–isobaric) ensemble was applied with a temperature of 300K and pressure of 1 bar. The simulation length was 100 ns, with relaxation time 1 ps. The force field parameters for each simulation were according to OPLS_2005 [63]. The long-range electrostatic interactions were calculated using the particle mesh Ewald (PME) method [64]. The cutoff radius in Coulomb interactions was 9.0 Å. The water molecules were described using a simple point charge model (SPC) [65]. The Martyna–Tuckerman–Klein chain coupling scheme [66] with a coupling constant of 2.0 ps was used for pressure control and the Nose–Hoover chain coupling scheme for temperature control. Nonbonded forces were calculated using an r-RESPA integrator, where the short-range forces were updated every step and the long-range forces were updated every three steps. The trajectories were saved at 4.8 ps intervals for analysis. To analyse the behaviour and interactions between the ligands and protein, we used the Simulation Interactions Diagram tool implemented in the Desmond molecular dynamics package.

Acknowledgements This research was supported by Basic Science Research Program through the National Research Foundation of Korea (NRF) funded by the Ministry of Education (NRF-2019R111A3A01059089).

Compliance with ethical standards

Conflict of interest The authors declare that they have no conflict of interest.

References

- Xue W, Warshawsky D (2005) Metabolic activation of polycyclic and heterocyclic aromatic hydrocarbons and DNA damage: A review. *Toxicol Appl Pharmacol* 206:73–93. <https://doi.org/10.1016/j.taap.2004.11.006>
- Romeo G, Chiacchio U, Corsaro A, Merino P (2010) Chemical synthesis of heterocyclic-sugar nucleoside analogues. *Chem Rev* 110:3337–3370. <https://doi.org/10.1021/cr800464r>
- Arora P, Arora V, Lamba HS, Wadhwa D (2012) Importance of heterocyclic chemistry: a review. *IJPSR* 3:2947–2954
- Gieg LM, Otter A, Fedorak PM (1996) Carbazole degradation by *Pseudomonas* sp. LD2: metabolic characteristics and the identification of some metabolites. *Environ Sci Technol* 30:575–585. <https://doi.org/10.1021/es950345v>
- Berry DF, Francis AJ, Bollagi JM (1987) Microbial metabolism of homocyclic and heterocyclic aromatic compounds under anaerobic conditions. *Microbiol Rev* 51:43–59

6. Vanjare BD, Mahajan PG, Dige NC, Phull AR, Kim SJ, Lee KH (2019) Synthesis and studies on photophysical properties of rhodamine derivatives for bioimaging applications. *Bull Kor Chem Soc* 40:554–559. <https://doi.org/10.1002/bkcs.11733>
7. Mahajan PG, Dige NC, Vanjare BD, Kamaraj E, Seo SY, Lee KH (2019) Nano molar level chromogenic and fluorogenic sensing of heavy metal ions using multi-responsive novel Schiff base as a dual mode chemosensor. *J Photochem Photobiol A* 385:112089. <https://doi.org/10.1016/j.jphotochem.2019.112089>
8. Bock VD, Speijer D, Hiemstra H, Maarseveen JHV (2007) 1,2,3-Triazoles as peptide bond isosteres: synthesis and biological evaluation of cyclotetrapeptide mimics. *Org Bio Chem* 5:971–975. <https://doi.org/10.1039/B616751A>
9. Schmiere H, Friebe J, Streube P, Hesse R, Kopsel R (1999) Change of chemical bonding of nitrogen of polymeric Nheterocyclic compounds during pyrolysis. *Carbon* 37:1965–1978. [https://doi.org/10.1016/S0008-6223\(99\)00071-8](https://doi.org/10.1016/S0008-6223(99)00071-8)
10. Hu Y, Li CH, Wang XM, Yang YH, Zhu HL (2014) 1,3,4-Thiadiazole: synthesis, reactions, and applications in medicinal, agricultural, and materials chemistry. *Chem Rev* 114:5572–5610. <https://doi.org/10.1021/cr400131u>
11. Li J, Wang D, Zhang Y, Li J, Chen B (2009) Facile one-pot synthesis of 4,5-disubstituted 1,2,3-(NH)-triazoles through sonogashira coupling/1,3-dipolar cycloaddition of acid chlorides, terminal acetylenes, and sodium azide. *Org Lett* 11:3024–3027. <https://doi.org/10.1021/ol901040d>
12. Liu Y, Yan W, Chen Y, Petersen JL, Shi X (2008) Efficient synthesis of N-2-aryl-1,2,3-triazole fluorophores via post-triazole arylation. *Org Lett* 10:5389–5392. <https://doi.org/10.1021/ol802246q>
13. Ma Y, Liu R, Gong X, Li Z, Huang Q, Wang H, Song G (2006) Synthesis and herbicidal activity of *N*, *N*-diethyl-3-(arylselenonyl)-1H-1,2,4-triazole-1-carboxamide. *J Agric Food Chem* 54:7724–7728. <https://doi.org/10.1021/jf0609328>
14. Blair LM, Sperry J (2013) Natural products containing a nitrogen–nitrogen bond. *J Nat Prod* 76:794–812. <https://doi.org/10.1021/np400124n>
15. Vanjare BD, Mahajan PG, Hassan M, Raza H, Seo SY, Hong SK, Lee KH (2018) Design, synthesis, photophysical properties, biological estimation and molecular docking studies of novel schiff base derivatives as potential urease inhibitors. *J Fluor* 28:1295–1304. <https://doi.org/10.1007/s10895-018-2289-1>
16. Banerjee S, Ganguly S, Sen KK (2013) A review on 1,2,4-triazoles. *J Adv Pharm Edu Res* 3:102–115
17. Xu M, Peng Y, Zhu L, Wang S, Ji J, Rakesh KP (2019) Triazole derivatives as inhibitors of Alzheimer's disease: current developments and structure-activity relationships. *Eur J Med Chem* 180:656–672. <https://doi.org/10.1016/j.ejmech.2019.07.059>
18. Palaska E, Sahin G, Kelicen P, Durlu NT, Altinok G (2002) Synthesis and anti-inflammatory activity of 1-acylthiosemicarbazides, 1,3,4-oxadiazoles, 1,3,4-thiadiazoles and 1,2,4-triazole-3-thiones. *Il Farmaco* 57:101–107. [https://doi.org/10.1016/S0014-827X\(01\)01176-4](https://doi.org/10.1016/S0014-827X(01)01176-4)
19. Holla BS, Veerendra B, Shivananda MK, Poojary B (2003) Synthesis characterization and anticancer activity studies on some Mannich bases derived from 1,2,4-triazoles. *Eur J Med Chem* 38:759–767. [https://doi.org/10.1016/S0223-5234\(03\)00128-4](https://doi.org/10.1016/S0223-5234(03)00128-4)
20. Ali KA, Ragab EA, Farghaly TA, Abdalla MM (2011) Synthesis of new functionalized 3-substituted [1,2,4] triazolo [4,3-a] pyrimidine derivatives: potential antihypertensive agents. *Acta Pol Pharma Drug Res* 68:237–247
21. Manohar S, Khan SI, Rawat DS (2011) Synthesis of 4-aminoquinoline-1,2,3-triazole and 4-aminoquinoline-1,2,3-triazole-1,3,5-triazine Hybrids as Potential Antimalarial Agents. *Chem Bio Drug Des* 78:124–136. <https://doi.org/10.1111/j.1747-0285.2011.01115.x>
22. Eswaran S, Adhikari AV, Shetty NS (2009) Synthesis and antimicrobial activities of novel quinoline derivatives carrying 1,2,4- triazole moiety. *Eur J Med Chem* 44:4637–4647. <https://doi.org/10.1016/j.ejmech.2009.06.031>
23. Kucukguzel I, Tatar E, Kucukguzel SG, Rollas S, Clercq ED (2008) Synthesis of some novel thiourea derivatives obtained from 5-[(4- aminophenoxy)methyl]-4-alkyl/aryl-2,4-dihydro-3H-1,2,4-triazole-3-thiones and evaluation as antiviral/anti-HIV and anti-tuberculosis agents. *Euro J Med Chem* 43:381–392. <https://doi.org/10.1016/j.ejmech.2007.04.010>
24. Brzozowski Z (1998) 2-Mercapto N-(AZOLYL) benzenesulfonamides. VI synthesis and anti-HIV activity of some new 2-mercapto-N-(1,2,4- Triazol-3-YL) Benzenesulfonamides derivatives containing the 1,2,4-Triazol moiety fused with a variety of hetero aromatic rings. *Acta Pol Pharma Drug Res* 55:473–480
25. Venkatarao V, Kumar L, Jhaa A, Sridhar G (2019) Synthesis and biological evaluation of chalcone fused quinoline derivatives as anticancer agents. *Chem Data Coll* 22:100236. <https://doi.org/10.1016/j.cdc.2019.100236>
26. Aher NC, Pore VS, Mishra NN, Kumar A, Shukla PK, Sharma A, Bhat MK (2009) Synthesis and antifungal activity of 1,2,3-triazole containing fluconazole analogues. *Bioorg Med Chem Lett* 19:759–763. <https://doi.org/10.1016/j.bmcl.2008.12.026>
27. Sujatha K, Shanthi G, Selvam NP, Manoharan S, Perumal PT, Rajendran M (2009) Synthesis and antiviral activity of 4,40-(arylmethylene) bis (1H-pyrazol-5-ols) against peste des petits ruminant virus (PPRV). *Bioorg Med Chem Lett* 19:4501–4503. <https://doi.org/10.1016/j.bmcl.2009.02.113>
28. Buzdar AU, Robertson JFR, Eiermann W, Nabholz J (2002) An overview of the pharmacology and pharmacokinetics of the newer generation aromatase inhibitors anastrozole, letrozole, and exemestane. *Cancer* 95:2006–2016. <https://doi.org/10.1002/cncr.10908>
29. Mokrosz JL, Duszynska B, Paluchowska MH, Minol SC, Mokrosz MJ (1995) A search for new trazodone-like antidepressants: synthesis and preliminary receptor binding studies. *Arch Pharm (Weinheim)* 328:623–625
30. Bekircan O, Ulker S, Mentese E (2015) Synthesis of some novel heterocyclic compounds derived from 2-[3-(4-chlorophenyl)-5-(4-methoxybenzyl)-4H-1,2,4 triazol-4-yl] acetohydrazide and investigation of their lipase and α -glucosidase inhibition. *J Enzyme Inhib Med Chem* 30:1002–1009. <https://doi.org/10.3109/14756366.2014.1003213>
31. Dige NC, Mahajan PG, Raza H, Hassan M, Vanjare BD, Hong H, Lee KH, Latip J, Seo SY (2019) Ultrasound mediated efficient synthesis of new 4-oxoquinazolin-3(4H)-yl furan- 2-carboxamides as potent tyrosinase inhibitors: Mechanistic approach through chemoinformatics and molecular docking studies. *Bioorg Chem* 92:103201. <https://doi.org/10.1016/j.bioorg.2019.103201>
32. Mahajan PG, Dige NC, Vanjare BD, Raza H, Hassan M, Seo SY, Kim CH, Lee KH (2019) Facile synthesis of new quinazolinone benzamides as potent tyrosinase inhibitors: Comparative spectroscopic and molecular docking studies. *J Mole Struc* 1198:126915. <https://doi.org/10.1016/j.molstruc.2019.126915>
33. Monzani E, Quinti L, Perotti A, Casella L, Gullotti M, Randaccio L, Geremia S, Nardin G, Faleschini P, Tabbi G (1998) Tyrosinase models. Synthesis, structure, catechol oxidase activity, and phenol monooxygenase activity of a dinuclear copper complex derived from a triamino pentabenzimidazole ligand. *Inorg Chem* 37:553–562. <https://doi.org/10.1021/ic970996n>
34. Fairhead M, Meyer LT (2012) Bacterial tyrosinases: old enzymes with new relevance to biotechnology. *New Biotech* 29:183–191. <https://doi.org/10.1016/j.nbt.2011.05.007>
35. Sendovski M, Kanteev M, Ben-Yosef VS, Adir N, Fishman A (2011) A first structures of an active bacterial tyrosinase

- reveal copper plasticity. *J Mol Biol* 405:227–237. <https://doi.org/10.1016/j.jmb.2010.10.048>
36. Ramsden CA, Riley PA (2014) Tyrosinase: the four oxidation states of the active site and their relevance to enzymatic activation, oxidation and inactivation. *Bioorg Med Chem* 22:2388–2395. <https://doi.org/10.1016/j.bmc.2014.02.048>
37. Ullah S, Kang D, Lee S, Ikram M, Park C, Park Y, Yoon S, Chun P, Moon HR (2019) Synthesis of cinnamic amide derivatives and their anti-melanogenic effect in α -MSH-stimulated B16F10 melanoma cells. *Eur J Med Chem* 161:78–92. <https://doi.org/10.1016/j.ejmech.2018.10.025>
38. Brenner M, Hearing VJ (2008) The protective role of melanin against UV damage in human skin. *Photochem Photobiol* 84:539–549. <https://doi.org/10.1111/j.1751-1097.2007.00226.x>
39. Chang T (2012) Natural melanogenesis inhibitors acting through the downregulation of tyrosinase activity. *Materials* 5:1661–1685. <https://doi.org/10.3390/ma5091661>
40. Bandgar BP, Adsul LK, Chavan HV, Shringare SN, Korbadi BL, Jalde SS, Lonikar SV, Nile SH, Shirfule AL (2012) Synthesis, biological evaluation, and molecular docking of N-[3-[3-(9-methyl-9H-carbazol-3-yl)-acryloyl]-phenyl]-benzamide/amide derivatives as xanthine oxidase and tyrosinase inhibitors. *Bioorg Med Chem* 20:5649–5657. <https://doi.org/10.1016/j.bmc.2012.07.001>
41. Xie W, Zhang H, He J, Zhang J, Yu Q, Luo C, Li S (2017) Synthesis and biological evaluation of novel hydroxybenzaldehyde based kojic acid analogues as inhibitors of mushroom tyrosinase. *Bioorg Med Chem Lett* 27:530–532. <https://doi.org/10.1016/j.bmcl.2016.12.027>
42. Xie W, Zhang J, Ma X, Yang W, Zhou Y, Tang X, Zou Y, Li H, He J, Xie S, Zhao Y, Liu F (2015) Synthesis and biological evaluation of kojic acid derivatives containing 1,2,4-triazole as potent tyrosinase inhibitors. *Chem Biol Drug Des* 86:1087–1092. <https://doi.org/10.1111/cbdd.12577>
43. Abbas Q, Raza H, Hassan M, Phull AR, Kim SJ, Seo SY (2017) Acetazolamide inhibits the level of tyrosinase and melanin: an enzyme kinetic, in vitro, in vivo, and in silico studies. *Chem Biodiv* 14(1–13):e1700117. <https://doi.org/10.1002/cbdv.201700117>
44. Lin LC, Chen CY, Kuo CH, Lin YS, Hwang BH, Wang TK, Kuo YH, Wang HMD (2018) 36H: a novel potent inhibitor for antimelanogenesis. *Oxid Med Cell Longev*. <https://doi.org/10.1155/2018/6354972>
45. Kang SM, Heo SJ, Kim KN, Lee SH, Yang HM, Kim AD, Jeon YJ (2012) Molecular docking studies of a phlorotannin, dieckol isolated from *Ecklonia cava* with tyrosinase inhibitory activity. *Bioorg Med Chem* 20:311–316. <https://doi.org/10.1016/j.bmc.2011.10.078>
46. Vontzalidou A, Zoidis G, Chaita E, Makropoulou M, Aligianis N, Lambrinidis G, Mikros E, Skaltsounis AL (2012) Design, synthesis and molecular simulation studies of dihydrostilbene derivatives as potent tyrosinase inhibitors. *Bioorg Med Chem Lett* 22:5523–5526. <https://doi.org/10.1016/j.bmcl.2012.07.029>
47. Lima CA, Silva JRA, Cardoso EDTC, Silva EO, Lameira J, Nascimento JLMD, Brasil DSB, Alves CN (2014) Combined kinetic studies and computational analysis on kojic acid analogs as tyrosinase inhibitors. *Molecules* 19:9591–9605. <https://doi.org/10.3390/molecules19079591>
48. Wagle A, Seong SH, Joung EJ, Kim HR, Jung HA, Choi JS (2018) Discovery of a highly potent tyrosinase inhibitor, luteolin 5-O- β -D-glucopyranoside, isolated from *Cirsium japonicum* var. *maackii* (Maxim.) Matsum., Korean thistle: kinetics and computational molecular docking simulation. *ACS Omega* 3:17236–17245. <https://doi.org/10.1021/acsomega.8b02694>
49. Butt ARS, Abbasi MA, Rehman A, Siddiqui SZ, Hassan M, Raza H, Shah SAA, Seo SY (2019) Synthesis and structure-activity relationship of elastase inhibiting novel ethylated thiazole-triazole acetamide hybrids: mechanistic insights through kinetics and computational contemplations. *Bioorg Chem* 86:197–209. <https://doi.org/10.1016/j.bioorg.2019.01.040>
50. Ghani U, Ullah N (2010) New potent inhibitors of tyrosinase: novel clues to binding of 1,3,4-thiadiazole-2(3H)-thiones, 1,3,4-oxadiazole-2(3H)-thiones, 4-amino-1,2,4-triazole-5(4H)-thiones, and substituted hydrazides to the dicopper active site. *Bioorg Med Chem* 18:4042–4048. <https://doi.org/10.1016/j.bmc.2010.04.021>
51. Abbas Q, Ashraf Z, Hassan M, Nadeem H, Latif M, Afzal S, Seo SY (2017) Development of highly potent melanogenesis inhibitor by in vitro, in vivo and computational studies. *Dru Des Dev Ther* 11:2029–2046
52. Saeed A, Mahesar PA, Channar PA, Abbas Q, Larik FA, Hassan M, Raza H, Seo SY (2017) Synthesis, molecular docking studies of coumarinyl-pyrazolinyl substituted thiazoles as non-competitive inhibitors of mushroom tyrosinase. *Bioorg Chem* 74:187–196. <https://doi.org/10.1016/j.bioorg.2017.08.002>
53. Larik FA, Saeed A, Channar PA, Muqadar U, Abbas Q, Hassan M, Seo SY, Bolte M (2017) Design, synthesis, kinetic mechanism and molecular docking studies of novel 1-pentanoyl-3-arylthioureas as inhibitors of mushroom tyrosinase and free radical scavengers. *Euro Jour Med Chem* 141:273–281. <https://doi.org/10.1016/j.ejmech.2017.09.059>
54. Song S, You A, Chen Z, Zhu G, Wen H, Song H, Yi W (2017) Study on the design, synthesis and structure-activity relationships of new thiosemicarbazone compounds as tyrosinase inhibitors. *Euro Jour Med Chem* 139:815–825. <https://doi.org/10.1016/j.ejmech.2017.08.033>
55. Shin NH, Ryu SY, Choi EJ, Kang SH, Chang IM, Min KR, Kim Y (1998) Oxyresveratrol as the potent inhibitor on dopa oxidase activity of mushroom tyrosinase. *Biochem Biophys Res Commun* 243:801–803. <https://doi.org/10.1006/bbrc.1998.8169>
56. Pettersen EF, Goddard TD, Huang CC, Couch GS, Greenblatt DM, Meng EC, Ferrin TE (2006) UCSF Chimera: a visualization system for exploratory research and analysis. *J Comput Chem* 25:1605–1612. <https://doi.org/10.1002/jcc.20084>
57. Lovell SC, Davis IW, Arendall WB, De Bakker PI, Word JM, Prisant MG, Richardson JS, Richardson DC (2002) Structure validation by Calpha geometry: phi, psi and Cbeta deviation. *Proteins* 50:437–450. <https://doi.org/10.1002/prot.10286>
58. Chen VB, Arendall WB III, Headd JJ, Keedy DA, Immormino RM, Kapral GJ, Murray LW, Richardson JS, Richardson DC (2010) MolProbity: all-atom structure validation for macromolecular crystallography. *Acta Cryst Sec D* 66:12–21. <https://doi.org/10.1107/S0907444909042073>
59. Studio Discovery (2008) version 2.1. San Diego, CA, Accelrys
60. Friesner RA, Murphy RB, Repasky MP, Frye LL, Greenwood JR, Halgren TA, Sanschagrin PC, Daniel TM (2006) Extra precision glide: docking and scoring incorporating a model of hydrophobic enclosure for protein-ligand complexes. *J Med Chem* 49:6177–6196. <https://doi.org/10.1021/jm051256o>
61. Farid R, Day T, Friesner RA, Pearlstein RA (2006) New insights about HERG blockade obtained from protein modeling, potential energy mapping, and docking studies. *Bioorg Med Chem* 14:3160–3173. <https://doi.org/10.1016/j.bmc.2005.12.032>
62. Bowers KJ, Chow E, Xu H, Dror RO, Eastwood MP, Gregersen BA, Klepeis JL, Kolossvary I, Moraes MA, Sacerdoti FD, Salmon JK, Shan Y, Shaw DE (2006) Scalable algorithms for molecular dynamics simulations on commodity clusters. *ACM/IEEE*. <https://doi.org/10.1109/SC.2006.54>
63. Banks JL, Beard HS, Cao Y, Cho AE, Damm W, Farid R, Felts AK, Halgren TA, Mainz DT, Maple JR, Murphy R, Philipp DM, Repasky MP, Zhang LY, Berne BJ, Friesner RA, Gallicchio E, Levy RM (2005) Integrated modeling program. Applied chemical theory (IMPACT). *J Comput Chem* 26:1752–1780. <https://doi.org/10.1002/jcc.20292>

64. Toukmaji AY, Board JA Jr (1996) Ewald summation techniques in perspective: a survey. *Comp Phys Comm* 95:73–92. [https://doi.org/10.1016/0010-4655\(96\)00016-1](https://doi.org/10.1016/0010-4655(96)00016-1)
65. Zielkiewicz J (2005) Structural properties of water: comparison of the SPC, SPCE, TIP4P, and TIP5P models of water. *J Chem Phys* 123:104501. <https://doi.org/10.1063/1.2018637>
66. Martyna GJ, Klein ML (1992) Nose-Hoover chains: the canonical ensemble via continuous dynamics. *J Chem Phys* 97:2635. <https://doi.org/10.1063/1.463940>

Publisher's Note Springer Nature remains neutral with regard to jurisdictional claims in published maps and institutional affiliations.